KOITER ASYMPTOTIC ANALYSIS OF THIN-WALLED COLD-FORMED STEEL MEMBERS

Viorel UNGUREANU[*,], Dan DUBINA[*,**], Andrei CRISAN[*], Antonio MADEO[***], Giuseppe ZAGARI[***], Giovanni ZUCCO[***], Raffaele ZINNO[***]**

[*]Faculty of Civil Engineering, Department of Steel Structures and Structural Mechanics, Politehnica University of Timisoara, Timisoara, Romania
[**]Laboratory of Steel Structures, Romanian Academy – Timisoara Branch, Timisoara, Romania
[***]MODELING Department, University of Calabria, Cosenza, Italy

viorel.ungureanu@upt.ro, dan.dubina@upt.ro, andrei crisan@upt.ro, antonio.madeo81@unical.it
giuseppe.zagari@unical.it, giovannizucco@gmail.com, raffaele.zinno@unical.it

received 6 September 2015, revised 11 December 2015, accepted 14 December 2015

Abstract: An imperfection sensitivity analysis of cold-formed steel members in compression is presented. The analysis is based on Koiter's approach and Monte Carlo simulation. If the modes interaction is correctly accounted, than the limit load and the erosion of critical buckling load can be easily evaluated. Thousands of imperfection can be analysed with very low computational cost and an effective statistical evaluation of limit performance can be carried out. The analysis is done on pallet rack uprights in compression, based on an intensive experimental study carried out at the Politehnica University of Timisoara.

Key words: Koiter Asymptotic Approach, Instability Problems, Thin-Walled Cold-Formed Steel Members, Imperfection Sensitivity Analysis, Monte Carlo

1. INTRODUCTION

The finite element implementation of Koiter's asymptotic approach allows to evaluate the pre-critical and initial post-critical behaviour of slender elastic structures, also in the presence of strong non-linear for pre-critical and in the case of interactive buckling (Casciaro, 2005). The method is considered very attractive for its advantages in respect to path-following approach (Riks, 1979). These consist in an accurate post-buckling analysis and in an efficient imperfection sensitivity analysis with low computational cost (Casciaro, 2005). The main difficulties arise in the availability of geometrically coherent structural model and in an accurate evaluation of their high order energy variations (Garcea et al., 2012a, 2012b). The use of co-rotational formulation, within a mixed formulation, allows to have a general finite element implementation of Koiter analysis (Zagari et al., 2013).

Our recent technology (Barbero et al., 2014, 2015), in terms of numerical implementation is applied for the evaluation of performance of slender cold-formed steel members especially for the case of modal interaction. In particular, an efficient and robust imperfection sensitivity analysis is performed. Using a Monte Carlo simulation, for a random sequence of imperfections assumed with the shape as linear combination of buckling modes, the equilibrium paths for the imperfect structures are recovered. The load carrying capacity is evaluated statistically. The worst imperfections are detected and the limit load is obtained, allowing the evaluation of erosion of critical bifurcation load (Dubina and Ungureanu, 2014).

2. THEORETICAL BACKGROUND

A summary of the FE asymptotic analysis proposed by Casciaro et al. is presented (Casciaro, 2005; Garcea et al., 2014a, 2014b). The described implementation is called quadratic algorithm. The method is based on the expansion of the potential energy, in terms of load factor λ and buckling mode amplitudes ξ_i, which is characterized by fourth-order accuracy. It provides an approximation of the equilibrium path by performing the following steps:

1. The fundamental path is obtained as a linear extrapolation, from a known equilibrium configuration:

$$u^f[\lambda] = \lambda\hat{u} \tag{1}$$

where u is the field of configuration variables in terms of stress and displacement and û is the tangent obtained as a solution of the linear equation

$$\Phi_0''\hat{u}\delta u = \hat{p}\delta u,\ \forall\delta u \in \mathcal{J} \tag{2}$$

where Φ'' is the strain energy while an index denotes the point along u^f which the quantities are evaluated, that is $\Phi_0'' \equiv \Phi''\left[u^f[\lambda_0]\right]$.

2. A cluster of buckling loads $\{\lambda_0 \dots \lambda_m\}$ and associated buckling modes $(\dot{v}_1 \dots \dot{v}_m)$ are defined along $u^f[\lambda]$ by the critical condition

$$\Phi''[u^f[\lambda_i]]\dot{v}_i\delta u = 0,\ \forall\delta u \in \mathcal{J}. \tag{3}$$

Buckling loads are considered to be sufficiently close to each other to allow the following linearization

$$\Phi_b''\dot{v}_i\delta u + (\lambda_i - \lambda_b)\Phi_b'''\hat{u}\dot{v}_i\delta u = 0,\ \forall\delta u \in \mathcal{J}. \tag{4}$$

λ_b being an appropriate reference value of λ (e.g. the first of λ_i or their mean value). Normalizing we obtain $\Phi_b'''\hat{u}\dot{v}_i\dot{v}_j = \delta_{ij}$, where δ_{ij} is Kroneker's symbol.

3. The tangent space $\mathcal{J}$ is decomposed into the tangent $\mathcal{V} \equiv \{\dot{v} = \sum_i \dot{v}_i\}$ and orthogonal $\mathcal{W} \equiv \{w : \Phi_b'''\hat{u}\dot{v}_i w = 0\}$ subspaces so that $\mathcal{J} = \mathcal{V} \oplus \mathcal{W}$. Denoting $\xi_0 = \lambda$ and

$\dot{v}_0 = \hat{u}$, the asymptotic approximation for the required path is defined by the expansion

$$u[\lambda, \xi_k] \equiv \sum_{i=0}^{m} \xi \dot{v}_i + \frac{1}{2}\sum_{i=0}^{m} \xi_i \xi_j w_{ij} \quad (5)$$

where w_{ij} are the quadratic corrections introduced to satisfy the projection of eqn. (1) onto $\mathcal{W}$ and obtained by the linear orthogonal equations

$$\Phi_b'' w_{ij} \delta w = -\Phi_b''' \dot{v}_i \dot{v}_j \delta w, w_{ij} \quad \delta w \in \mathcal{W} \quad (6)$$

where, because of the orthogonality condition, $w_{0i} = 0$.

4. The following energy terms are computed for $i, j, k = 1 \ldots m$:

$$\mu_k[\lambda] = \frac{1}{2}\lambda^2 \Phi_b''' \hat{u}^2 \dot{v}_k + \frac{1}{6}\lambda^2(\lambda - 3\lambda_b)\Phi_b''' \hat{u}^3 \dot{v}_k$$

$$A_{ijk} = \Phi_b''' \dot{v}_i \dot{v}_j \dot{v}_k \quad (7)$$

$$B_{ijhk} = \Phi_b'''' \dot{v}_i \dot{v}_j \dot{v}_h \dot{v}_k - \Phi_b'' \left(w_{ij} w_{hk} + w_{ih} w_{jk} + w_{ik} w_{jh}\right)$$

$$B_{00jk} = \Phi_b'''' \hat{u}^2 \dot{v}_i \dot{v}_k - \Phi_b'' w_{00} w_{ik}$$

$$B_{0ijk} = \Phi_b'''' \hat{u} \dot{v}_i \dot{v}_j \dot{v}_k$$

$$C_{ik} = \Phi_b'' w_{00} w_{ik}$$

where the implicit imperfection factors μ_k are defined by the 4th order expansion of the unbalanced work on the fundamental (i.e. $\mu_k[\lambda] = (\lambda \hat{p} - \Phi'[\lambda \hat{u}])\dot{v}_k$).

5. The equilibrium path is obtained by satisfying the projection of the equilibrium eqn. (1) onto $\mathcal{V}$. According to eqns. (7) and (8), we have

$$(\lambda_k - \lambda)\xi_k - \lambda_b \left(\lambda - \frac{\lambda_b}{2}\right)\sum_{i=1}^{m} \xi_i C_{ik} + \frac{1}{2} \sum_{i,j=1}^{m} \xi_i \xi_j A_{ijk} + \frac{1}{2}(\lambda - \lambda_b)^2 \sum_{i=1}^{m} \xi_i B_{00ik} + \frac{1}{2}(\lambda - \lambda_b) \sum_{i,j=1}^{m} \xi_i \xi_j B_{0ijk} + \frac{1}{6} \sum_{i,j,k=1}^{m} \xi_i \xi_j \xi_h B_{ijhk} + \mu_k[\lambda] = 0, \quad k = 1 \ldots m \quad (8)$$

Equation (8) corresponds to a highly nonlinear system in the m+1 unknowns, $-\xi_i$, and can be solved using a standard path-following strategy. It provides the initial post-buckling behaviour of the structure including modal interactions and jumping-after-bifurcation phenomena (see Fig. 1).

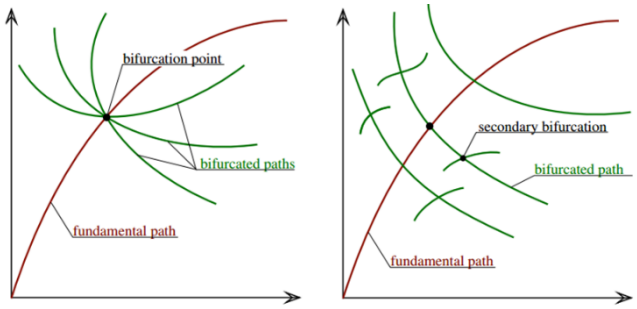

Fig. 1. Interactive buckling for coincident/nearly coincident buckling loads

In the analysis of thin-walled members the characterization of imperfection is often difficult. The presence of imperfections changes some aspects of structural response and often causes an erosion of the load carrying capacity, especially in the interactive buckling range. In the asymptotic algorithm the presences of imperfections expressed by a load $\tilde{p}[\lambda]$ and/or an initial displacement $\tilde{u}$, affect eqn. (9) only with the imperfection term $\mu_k[\lambda]$ that becomes (Casciaro, 2005).

$$\mu_k[\lambda] = \frac{1}{2}\lambda^2 \Phi_b''' \hat{u}^2 \dot{v}_k + \frac{1}{6}\lambda^2(\lambda - 3\lambda_b)\Phi_b''' \hat{u}^3 \dot{v}_k + \lambda \phi''' \tilde{u} \hat{u} \dot{v}_k - \tilde{p} \dot{v}_k \quad (9)$$

The aim of the imperfection sensitivity analysis is to link the presence of geometrical and load imperfections to the reduction in the limit load. For structures presenting coupled buckling even a small imperfection in loading or geometry can represent a significant reduction in ultimate load with respect to the bifurcation load (Garcea et al., 2014a, 2014b). So an effective safety analysis should include an investigation of all possible imperfection shapes and sizes to identify the worst imperfection cases.

3. NUMERICAL RESULTS

On the following, an imperfection sensitivity analysis for upright pallet racks in compression, with and without perforations, is presented. The geometry of the cross-section is shown in Fig. 2, while details related to cross-section, perforations, lengths, material, experimental tests and numerical simulations can be found in (Crisan et al., 2012a, 2012b). The member will be denoted on the following as RS125×3.2, as in (Crisan et al., 2012a, 2012b). The RS125×3.2 specimen has a perforated-to-brut cross-section ratios, A_N/A_B, of 0.806.

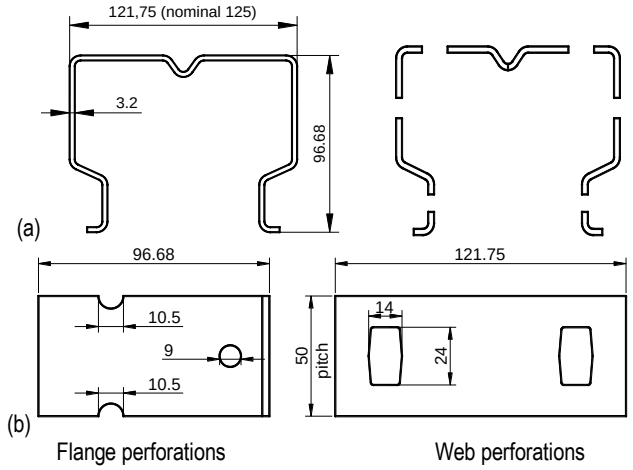

Fig. 2. (a) Geometry of RS125×3.2 section with and without perforations (dimensions are expressed in mm); (b) Perforations details

In this study, different lengths have been analysed and for each length imperfection sensitivity analyses have been performed. The minimum length considered was L = 1400 mm and the maximum one L = 2500 mm. Increments of 100 mm have been considered. The lengths range has been establish in order to include the interactive buckling range, computed based on ECBL approach (Dubina, 2001), considering the interaction of distortional and flexural buckling modes. The procedure was detailed in (Crisan et al., 2012a, 2012b).

In the imperfection sensitivity analysis only geometrical imper-

fections have been considered. In particular, the total imperfection $\tilde{u}$, as shown in eqn. (10), is assumed to be:

$$\tilde{u} = \tilde{u}^g + \tilde{u}^d \tag{10}$$

where $\tilde{u}^g$ and $\tilde{u}^d$ are the global and distortional/local imperfections, that are assumed as linear combinations of global $\dot{v}_i^g$ and distortional/local $\dot{v}_i^d$ buckling modes, that is:

$$\tilde{u}^g = \sum_i r_i \, \dot{v}_i^g \;\; i = 1..m^g$$
$$\tilde{u}^d = \sum_i r_i \, \dot{v}_i^d \;\; i = 1..m^d \tag{11}$$

In eqn. (11) r_i are random number, while m^g and m^d are the number of global and distortional/local buckling modes. The maximum values of $\tilde{u}^g_{max}$ and $\tilde{u}^d_{max}$ are assumed to be smaller than the assumed tolerances (see Fig. 3), i.e. $\tilde{u}^g_{max} < L/1000$ for global imperfection and $\tilde{u}^d_{max} < 1.5\,t$ for distortional one, where L and t are the length of the upright pallet rack and the thickness of the cross-section.

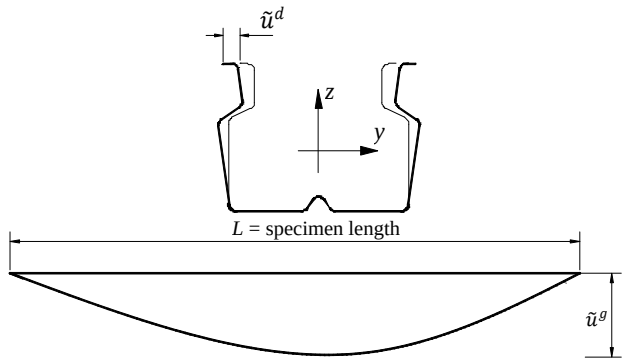

Fig. 3. Distortional and global imperfections for numerical analysis

For each length, the first four buckling modes are considered. For the simulation the rack was considered pinned at one end and simply supported at the other one. For the pinned end, all three translations together with rotation along the longitudinal axis were restrained. For the simply supported end, the translation along the section axis together and the torsional rotations were restrained. The details of the mesh are reported in Fig. 4.

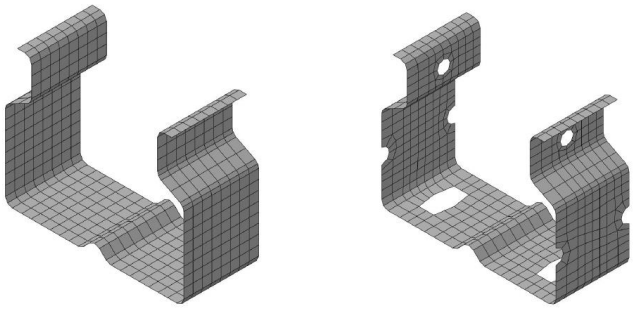

Fig. 4. Details of the mesh for RS125×3.2 brut and net section

For the range of lengths under evaluation, eight distortional buckling modes and two global buckling modes have been detected as shown in Tabs. 1 and 2 and Figs. 5 and 6.

It is easy to observe from Tables 1 and 2 that the interactive buckling range is between (2000 … 2500) mm, confirming the values obtained in (Crisan et al., 2012a).

Tab. 1. The first four buckling loads corresponding to the investigated lengths for RS125×3.2 brut section

L (mm)	λ_1 [kN]	Mode	λ_2 [kN]	Mode	λ_3 [kN]	Mode	λ_4 [kN]	Mode
1400	507.2	d_1	532.6	d_2	713.0	d_3	748.0	d_4
1500	505.6	d_1	509.7	d_2	696.8	d_4	698.6	d_3
1600	492.7	d_2	504.9	d_1	663.1	d_4	686.3	d_3
1700	481.1	d_2	501.6	d_1	643.1	d_4	677.5	d_3
1800	473.8	d_2	494.4	d_6	635.6	d_4	652.4	d_5
1900	470.0	d_2	484.8	d_6	611.6	d_4	632.3	d_5
2000	468.5	d_2	475.2	d_6	563.7	e_1	593.0	d_5
2100	467.0	d_6	468.2	d_7	516.2	e_1	550.0	e_2
2200	460.7	d_6	467.6	d_7	473.4	e_1	509.3	e_2
2300	435.1	e_1	456.4	d_6	465.9	d_7	471.9	e_2
2400	401.2	e_1	437.9	e_2	453.8	d_6	462.4	d_8
2500	370.9	e_1	407.1	e_2	452.6	d_6	458.0	d_8

Tab. 2. The first four buckling loads corresponding to the investigated lengths for RS125×3.2 net section

L (mm)	λ_1 [kN]	Mode	λ_2 [kN]	Mode	λ_3 [kN]	Mode	λ_4 [kN]	Mode
1400	441.8	d_1	474.3	d_2	627.9	d_3	652.4	d_4
1500	438.6	d_1	452.9	d_2	610.1	d_3	626.3	d_5
1600	436.1	d_2	438.0	d_1	589.3	d_5	597.5	d_3
1700	423.8	d_2	437.0	d_1	564.7	d_5	586.9	d_3
1800	415.4	d_2	433.4	d_1	551.7	d_5	573.2	d_3
1900	410.2	d_2	426.9	d_7	546.5	d_6	547.4	d_3
2000	407.6	d_2	419.0	d_7	504.7	e_1	516.3	d_3
2100	406.6	d_2	411.3	d_7	463.2	e_1	480.5	e_2
2200	404.8	d_7	406.4	d_2	425.3	e_1	446.0	e_2
2300	391.3	e_1	399.8	d_2	406.0	d_2	413.9	e_2
2400	360.9	e_1	384.5	e_2	396.3	d_7	404.4	d_2
2500	333.8	e_1	357.7	e_2	394.2	d_7	401.6	d_8

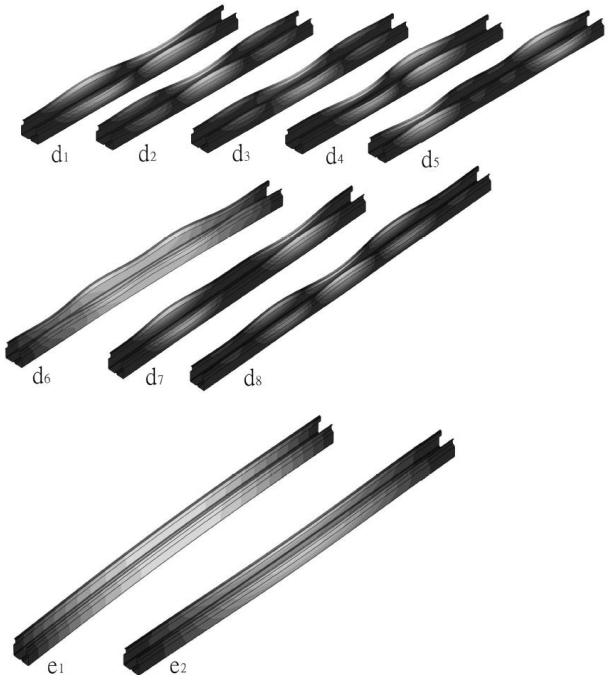

Fig. 5. Distortional d_1, d_2 ... d_8 and global e_1, e_2 buckling modes for RSB125×3.2 brut section in the range *L* = 1400 ... 2500 mm

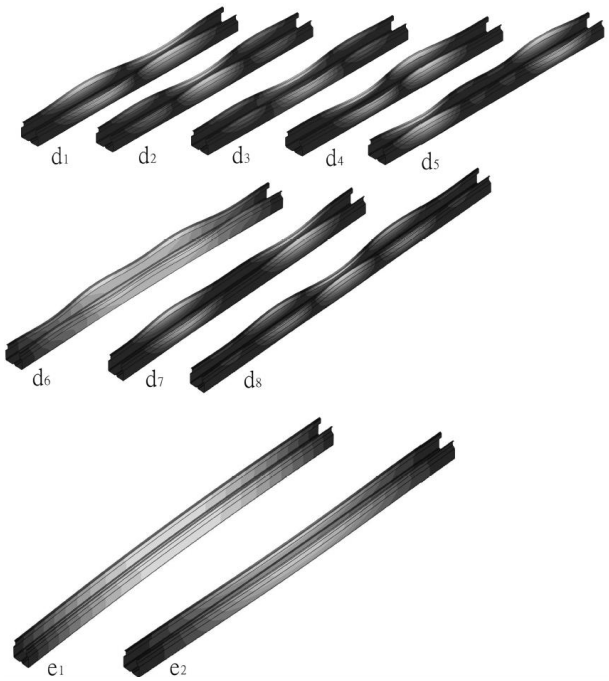

Fig. 6. Distortional d_1, d_2 ... d_8 and global e_1, e_2 buckling modes for RSN125×3.2 net section in the range L = 1400 ... 2500 mm

Fig. 7 presents the buckling loads versus the lengths of the upright members with and without perforations. The range corresponding to global/distortional interactive buckling can be clearly seen, as stated above.

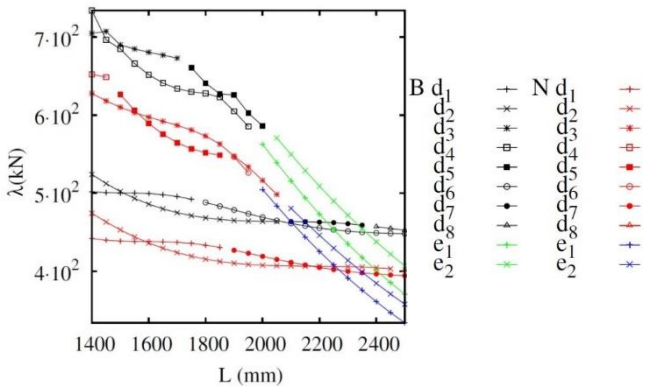

Fig. 7. Bucking load vs. corresponding length for the R125×3.2 brut (B) and net (N) sections

Fig. 8 presents the first four buckling modes for the 2200 mm length, while Fig. 9 the quadratic corrections for the same length, as was defined by eqn. (5). Note that, the aim of the paper is to find the worst imperfection case. Then, the real shape of the imperfection is not required and only the linear combinations of buckling modes are considered. Anyway, the validation of numerical model has been done according to the measured data in (Crisan et al., 2012a).

On the second step, the post-buckling analysis has been performed considering the four buckling modes presented in Tabs. 1 and 2, for the members with lengths L = 1400 ... 2500 mm. The changing of the buckling load and shape at varying lengths is shown in Fig. 5 for brut cross-sections and Fig. 6 for the section with perforations.

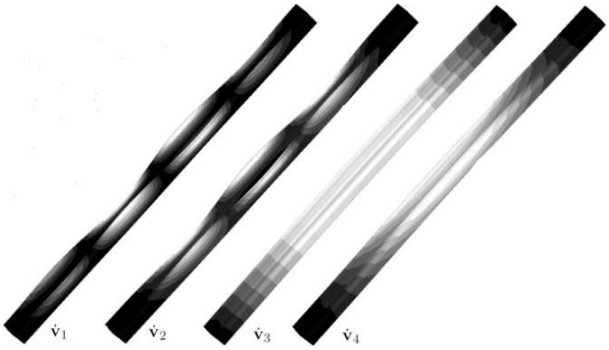

Fig. 8a. Buckling modes for the brut section with length of 2200 mm

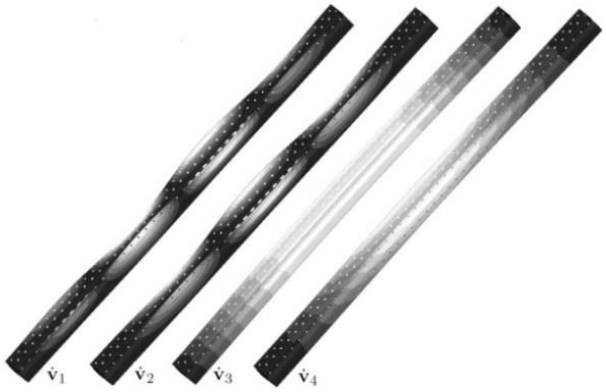

Fig. 8b. Buckling modes for the net section with length of 2200 mm

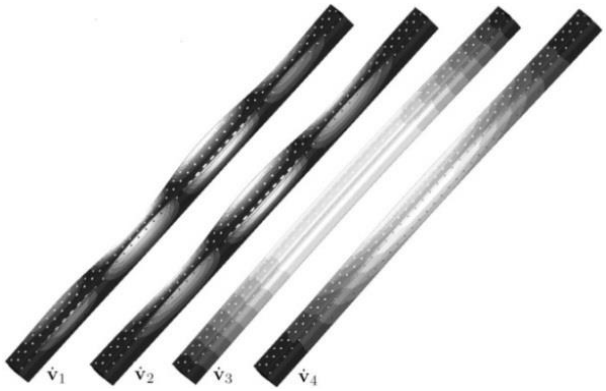

Fig. 9a. Quadratic corrections for the brut section with length of 2200 mm

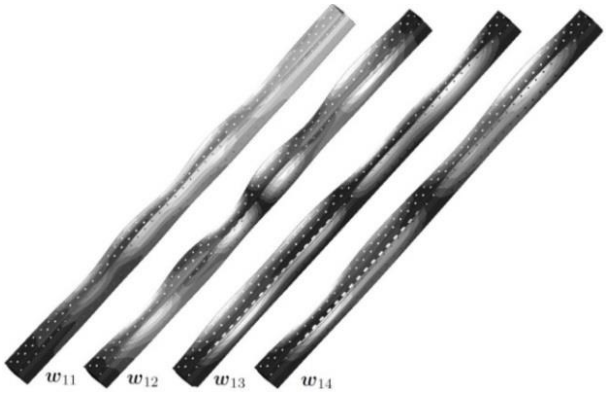

Fig. 9b. Quadratic corrections for the brut section with length of 2200 mm

The multimodal analysis has been performed considering the four buckling modes presented above. Five hundred random

geometric imperfections have been generated with a very low computational cost. The results, in terms of limit load/ displacements, for both brut and net cross-section, are shown in Fig. 10, while the worst imperfections and limit load shapes, for the length L = 2200 mm, are shown in Fig. 11.

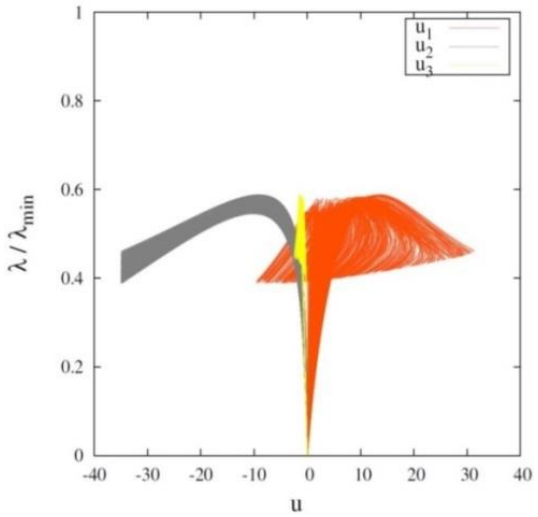

Fig. 10a. Brut section RS125×3.2 with length of 2200 mm: equilibrium paths λ versus u. The displacement components u_1, u_2 and u_3 are measured in the point of the middle of the upright pallet rack section

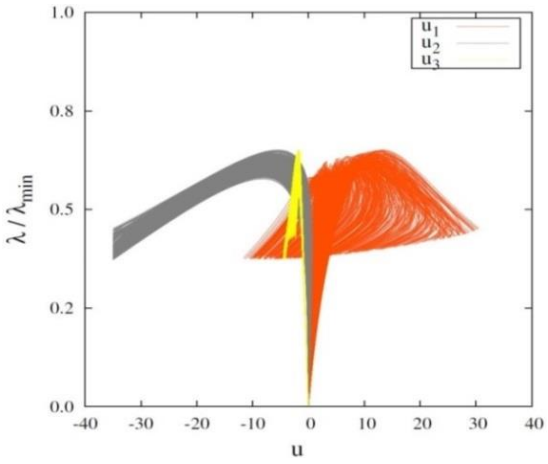

Fig. 10b. Net section RS125×3.2 with length of 2200 mm: equilibrium paths λ versus u. The displacement components u_1, u_2 and u_3 are measured in the point of the middle of the upright pallet rack section

The frequency for the limit loads and its probability distribution are reported in Fig. 12 (a and b). For the specimens with strong buckling interaction, the values are very close to the peak of the distribution. The length with strong interaction are also clearly highlighted, i.e. L = 2200 mm.

The average time required for the steps 1 to 4 have been studied (Barbero et al, 2015), and they remain of the order of seconds. This could allow users to run Monte Carlo simulations to account for other types of imperfections, i.e. load imperfection, residual stress, a.s.o., in order to obtain even more realistic evaluations of structural performance.

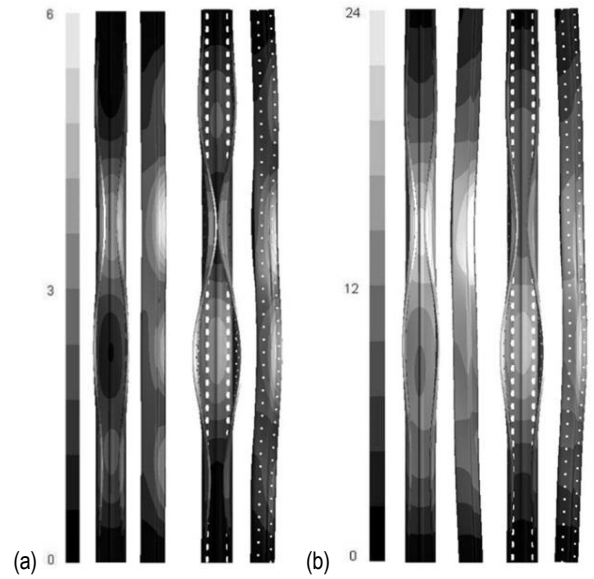

Fig. 11. Section RS125×3.2, brut and net, with the length of 2200 mm: (a) initial shapes for worst imperfection amplified by factor 5.0, (b) deformed shapes at limit load for worst imperfection amplified factor 2.5

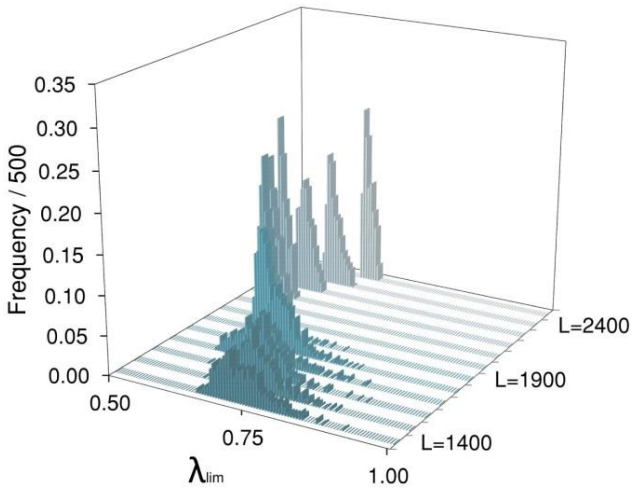

Fig. 12a. Frequency distribution of the limit load found λ_{lim} for the RS125×3.2 brut section

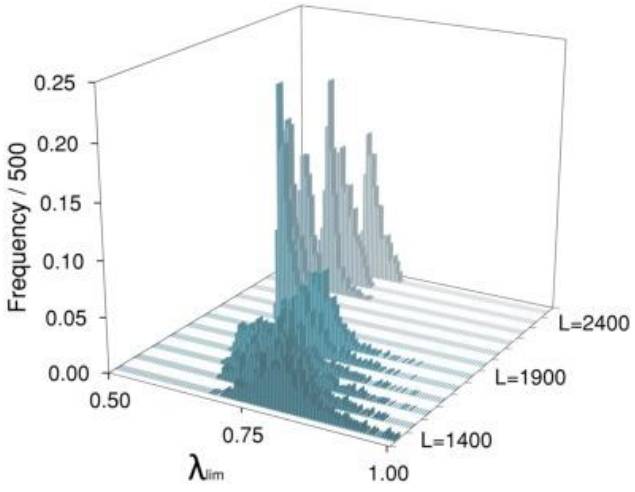

Fig. 12b. Frequency distribution of the limit load found λ_{lim} for the RS125×3.2 net section

4. EVALUATION OF ψ EROSION FACTORS

It is very well known that in the case of an ideal structure, the theoretical equilibrium bifurcation point and corresponding load, N_{cr}, are observed at the intersection of the pre-critical (primary) force-displacement curve with the post-critical (secondary) curve (see Fig. 13). For a real structure, affected by a generic imperfection, δ_0, the bifurcation point does not appear anymore and, instead, the equilibrium limit point is the one characterizing the ultimate capacity, N_u, of the structure. The difference between N_{cr} and N_u represents the *Erosion of the Critical Bifurcation Load*, due to the coupling and imperfections (Dubina, 2001).

In almost all practical cases, the mode interaction, obtained by coupling of a local instability with an overall one, is a result of design (e.g. calibration by design of mechanical and geometrical properties of member), and has a nonlinear nature.

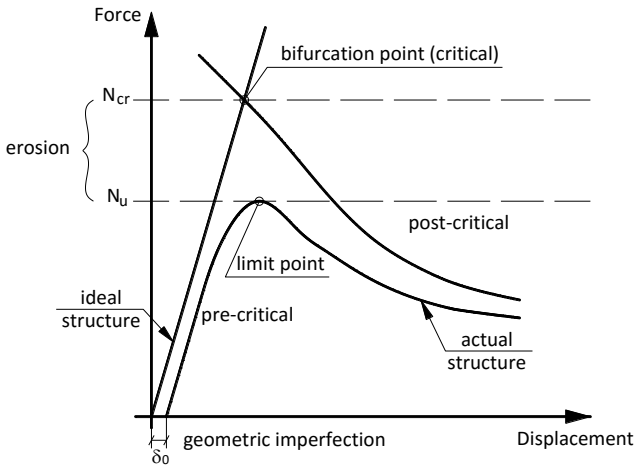

Fig. 13. Critical and post-critical behaviour

Due to the imperfections, an interaction erosion of critical bifurcation load occurs. This erosion is maximum in the coupling point vicinity. For members, an interactive slenderness range, in which sensitivity to imperfections is increased, may be identified. Depending on imperfection sensitivity, classes of interaction types, characterized by specific levels of erosion intensity, may be defined (Gioncu, 1994).

Being given a member in compression let assume two simultaneous buckling modes which might couple (see Fig. 14).

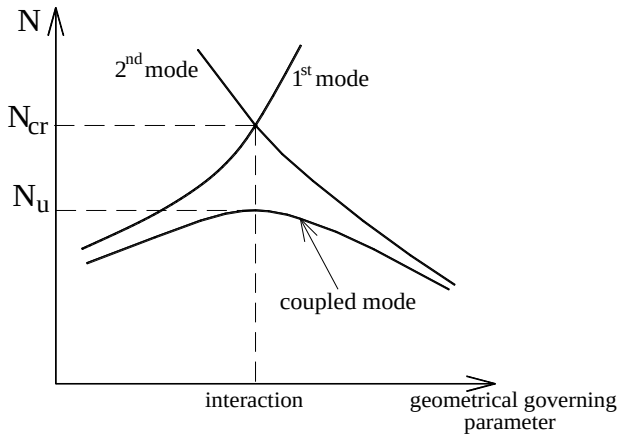

Fig. 14. Critical and post-critical behaviour

The perfect member is prone to interactive buckling, with the critical buckling load, N_{cr}, while the actual member with the ultimate load, N_u. The erosion coefficient, ψ, can be expressed as follows:

$$\psi = 1 - \bar{N}_u / \bar{N}_{cr} \tag{12}$$

and

$$\bar{N}_u = (1 - \psi)\bar{N}_{cr} \tag{13}$$

The Monte Carlo simulation also allows to found the worst imperfection case, as shown in Fig. 10, and to evaluate the erosion as shown in Fig. 15 (Dubina, 2001). The load carrying capacity is evaluated statistically. The worst imperfections are detected and the limit load is obtained so allowing the evaluation of erosion of critical bifurcation load according to eqn. (10). The evaluation of erosion is shown in Fig. 15. The maximum erosion has been detected for the specimens corresponding to the length L = 2200 mm.

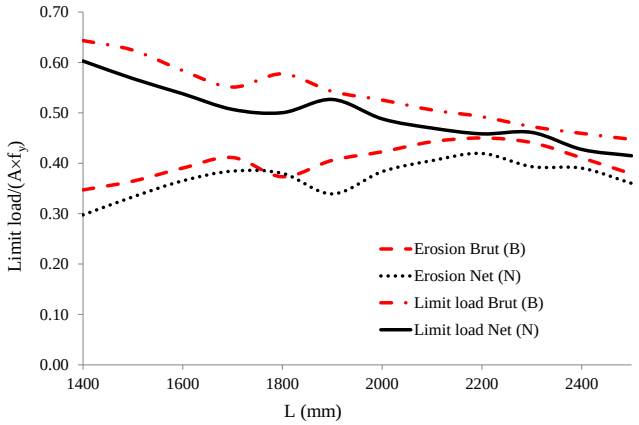

Fig. 15. The minimum limit load normalized to the cross-section capacity for brut (B) and net (N) section

The buckling modes that provide the maximum erosion and their participation are presented in Tab. 3. In Figs. 5 and 6 are defined these buckling modes.

Tab. 3. Buckling modes defining the maximum erosion and their participation, both for RS125×3.2 brut (B) and net (N) cross-section

	RS125×3.2 brut		RS125×3.2 net	
	Mode	% mode brut	Mode	% mode net
distortional	d6	99.23	d7	98.62
	d7	0.77	d2	1.38
global	e1	93.97	e1	89.08
	e2	6.03	e2	10.92

Once, evaluated the worst imperfections the sensitivity curves have been recovered (see Fig. 15). The figure shows that brut sections have a higher limit load than the net sections, however the slope of sensitivity curves is the same.

Finally, it can be observed that based on the above parametric study, the obtained maximum erosion are of 0.45 for the brut section (B) and 0.42 for the net section (N). In a direct comparison with the results obtained via ECBL approach (Dubina, 2001), it

can be observed they are in a good agreement with the ones obtained by Ungureanu and Dubina (2013), i.e. of 0.44 for the net section, but for a combination of imperfections ($\tilde{u}^{g}_{max} = \mathrm{L}/750$ and $\tilde{u}^{d}_{max} = 1.5$ t). The erosions obtained by Crisan et al. (2012b) via ECBL approach, i.e. 0.387 for the brut section and 0.395 for the net section, are also close to the ones presented above but have been obtained for different combination of imperfections, i.e. ($\tilde{u}^{g}_{max} = \mathrm{L}/1000$ and $\tilde{u}^{d}_{max} = 1$ t).

5. CONCLUSIONS

An imperfection sensitivity analysis using Koiter's approach and the Monte Carlo method has been applied for the evaluation of imperfection sensitivity of cold-formed upright members for pallet racks in compression, with and without perforations. The analysis allows to evaluate the limit loads, the erosion of the theoretical buckling due to both imperfections and the mode interaction. The main strengths of the proposed methodology are the ability to analyse thousands of random imperfections in a short time, with very low computational cost, to find the worst imperfections and to provide an accurate evaluation of the limit load and of the erosion of buckling load, with respect to theoretical case, due to buckling mode interaction.

Once again is shown and validated that the ECBL approach is an excellent and practical method that allows for the evaluation of ψ erosion coefficients and α imperfection factors, as result of interactive buckling.

REFERENCES

1. **Barbero E.J., Madeo A., Zagari G., Zinno R., Zucco G.** (2014), Koiter asymptotic analysis of folded laminated composite plates, *Composites Part B: Engineering*, 61, 267–274.
2. **Barbero E.J., Madeo A., Zagari G., Zinno R., Zucco G**. (2015), Imperfection sensitivity analysis of laminated folded plate, *Thin-Walled Structures*, 90, 128-139.
3. **Casciaro R.** (2005), *Computational asymptotic post-buckling analysis of slender elastic structures*, in *Phenomenological and Mathematical Modelling of Structural Instabilities*, M. Pignataro, V. Gioncu (eds.), Vol. 470, CISM International Centre for Mechanical Sciences, Springer Vienna, 95–276, 2005.
4. **Crisan A, Ungureanu V., Dubina D.** (2012a), Behaviour of cold-formed steel perforated sections in compression: Part 1-Experimental investigations, *Thin-Walled Structures*, 61, 86-96.
5. **Crisan A, Ungureanu V., Dubina D.** (2012b), Behaviour of cold-formed steel perforated sections in compression: Part 2-Numerical investigations and design considerations, *Thin-Walled Structures*, 61, 97-105.
6. **Dubina D.** (2001), The ECBL approach for interactive buckling of thin-walled steel members, *Steel Composite Structures*, 1(1), 75-96.
7. **Dubina D., Ungureanu V.** (2002), Effect of imperfections on numerical simulation of instability behaviour of cold-formed steel members, *Thin-Walled Structures*, 40(3), 239–262.
8. **Dubina D., Ungureanu V.** (2014), Instability mode interaction: from Van Der Neut model to ECBL approach, *Thin-Walled Structures*, 81, 39–49.
9. **Garcea G., Bilotta A., Madeo A., Casciaro R.** (2014a), Direct Evaluation of the Post-Buckling Behavior of Slender Structures Through a Numerical Asymptotic Formulation, *Direct Methods for Limit States in Structures and Materials*, Springer Netherlands, 203-228.
10. **Garcea G., Bilotta A., Madeo A., Zagari G., Casciaro R.** (2014b), A Numerical Asymptotic Formulation for the Post-buckling Analysis of Structures in Case of Coupled Instability, *Special Issue Stability And Nonlinear Analysis Of Steel Structures – Research Advances, Romanian Journal of Technical Sciences Applied Mechanics*, 59(1–2), 38-55.
11. **Garcea G., Madeo A., Casciaro R.** (2012a), The implicit corotational method and its use in the derivation of nonlinear structural models for beams and plates, *Journal of Mechanics of Materials and Structures*, 7(6), 509-538.
12. **Garcea G., Madeo A., Casciaro R.** (2012b), Nonlinear FEM analysis for beams and plate assemblages based on the implicit corotational method, *Journal of Mechanics of Materials and Structures*, 7(6), 539-574.
13. **Gioncu V.** (1994), General Theory of Coupled Instability, *Thin-Walled Structures (Special Issue on Coupled Instability in Metal Structures – CIMS'92)*, 19(2-4), 81-128.
14. **Riks E**. (1979), An incremental approach to the solution of snapping and buckling problems, *International Journal of Solids and Structures*, 15(7), 529–551, 1979.
15. **Ungureanu V., Dubina D.** (2013), Sensitivity to imperfections of perforated pallet rack sections, *Mechanics and Mechanical Engineering*, Lodz University of Technology, 17(2), 209–222.
16. **Zagari G., Madeo A., Casciaro R., de Miranda S., Ubertini F.** (2013), Koiter analysis of folded structures using a corotational approach, *International Journal of Solids and Structures*, 50(5), 755–765.

Special recognition is due to Prof. Raffaele Casciaro for his suggestions and comments. The authors from University of Calabria wish to acknowledge the International Network for the Exchange of Good Practices in Innovative, Seismically Safe and Eco-friendly Buildings (POR-FSE CALABRIA 2007-2013 RISPEISE) for the financial support. This work was partially supported by the strategic grant POSDRU/159/1.5/S/137070 (2014) of the Ministry of National Education, Romania, co-financed by the European Social Fund – Investing in People, within the Sectoral Operational Programme Human Resources Development 2007-2013."